Grain boundary mediated oxidation and interlayer dipolar coupling in a magnetic tunnel junction structure

J. W. Freeland, D. J. Keavney, R. Winarski, and P. Ryan
Advanced Photon Source, Argonne National Laboratory, Argonne, Illinois 60439

J. M. Slaughter, R. W. Dave, and J. Janesky
Motorola Labs, Physical Sciences Research Labs, Tempe, Arizona 85284

(Received 8 October 2002; revised manuscript received 17 January 2003; published 9 April 2003)

We present a study detailing changes in the layers of a magnetic tunnel junction that has been overoxidized to explore the impact of unwanted oxidation. From the evidence of grain boundary diffusion, we conclude that the microstructure plays an important role in determining the impact of the oxidation process. Layer-dependent switching measurements show that the change in the tunneling magnetoresistance was solely due to modified dipolar coupling after field annealing into the exchange biased state. This was confirmed by scattering measurements, which show clearly that the preanneal and postanneal interfacial structure remains unchanged.

DOI: 10.1103/PhysRevB.67.134411 PACS number(s): 85.70.Kh, 75.70.Cn, 78.70.Dm

Magnetic tunnel junctions (MTJ's) are the basis of the next generation of magnetic devices [e.g., nonvolatile magnetic random access memory (MRAM)] due to the high values of attainable tunneling magnetoresistance (TMR).[1,2] One issue of key importance is the formation of a high-quality insulating oxide spacer without influencing the quality of neighboring ferromagnetic contacts. Previous x-ray photoelectron (XPS) and x-ray absorption studies have looked at the oxidation of the Al spacer, as well as the impact of the oxidation process, on neighboring layers.[3–6] Evidence was found for oxidation of ferromagnetic contacts, which can be reduced by annealing.[5,6] Electron microscopy studies have shown that the oxidation of the Al spacer takes place by grain boundary diffusion of oxygen around the grain, which then moves into the grain.[7,8] This was first proposed to explain XPS studies of junction formation.[3,4] However, questions remain as to the exact structure of the interfacial oxide and its effect on the spin polarized tunneling in MTJ's.

In this article, we present a study of forced oxidation of ferromagnetic contacts in magnetic tunnel junctions to aid in understanding the mechanism of unwanted oxidation and the resulting impact on the magnetic properties. Our results show that the oxide moves into the bottom ferromagnetic contact via grain boundary diffusion and does not completely oxidize the interface with the Al oxide. In this way nonzero TMR can be observed even with the presence of some Co oxide at the interface. A large increase in TMR after field annealing is ascribed to changes in the dipolar interaction between the layers, while roughness studies show the structure was unaffected by the annealing process.

The samples consisted of an MTJ with a wedge-shaped Al oxide insulating layer (see Fig. 1). The plasma oxidation conditions favored creation of a 9 Å Al_2O_3 layer and therefore results in an overoxidized region at the thin end for use to study the mechanism by which the oxide moves into the bottom layer. The full structure is SiO_2/IrMn/CoFe (30 Å)/Al oxide wedge (5–9 Å)/NiFeCo(25 Å)/TaN(30 Å). A second half junction sample was made without the NiFeCo layer to clearly separate effects due to the CoFe layer. The films were ion beam deposited on 150 mm silicon wafers coated with 2000 Å of SiO_2. During deposition of the tunnel-barrier aluminum, the wafer was positioned at an angle to the incident sputtered flux, giving rise to a thickness variation across the wafer of approximately a factor of 2. The wafer was rotated during deposition of the other materials to produce layers with uniform thickness. The wafers were transferred in high vacuum to a second chamber where oxidation of the tunnel-barrier Al was performed with a uniform oxygen/argon plasma. Thus the tunnel barrier has varying Al thickness across the wafer but constant oxidation dose. The deposition rates were calibrated by x-ray reflectivity (XRR) and the deposition controlled with deposition time. The thickness profile of the aluminum wedge was determined by measuring the step height of a thick patterned film at many positions across the wafer diameter with an XRR-calibrated atomic force microscope.

Experiments were performed at sector 4 of the Advanced Photon Source.[9] The intermediate energy beamline (4-ID-C) provides high-resolution polarized x rays in the intermediate x-ray range of 500–3000 eV.[10] The x rays are generated by a novel circularly polarized undulator that provides left- and

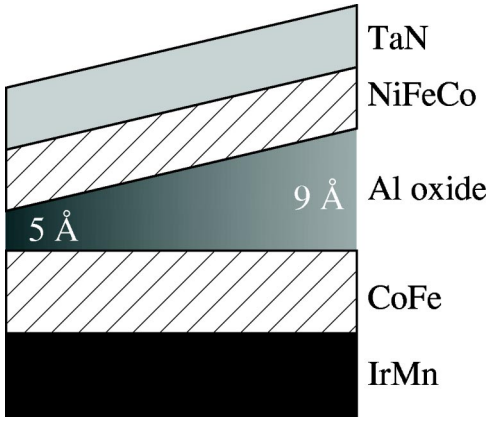

FIG. 1. Wedge shaped sample structure. The Al layer was plasma oxidized for an optimal thickness of 9 Å, which leads to an overoxidized region at the thin end of the wedge.

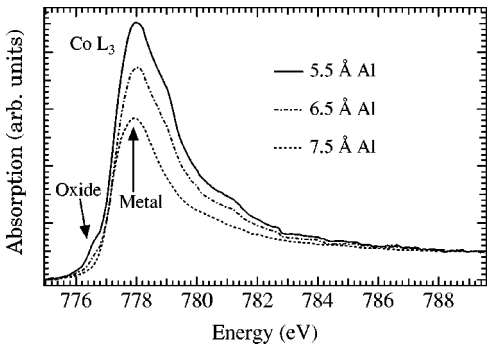

FIG. 2. Co L_3 absorption edge as a function of Al spacer thickness showing the formation of interfacial oxide at the $CoFe/Al_2O_3$ boundary.

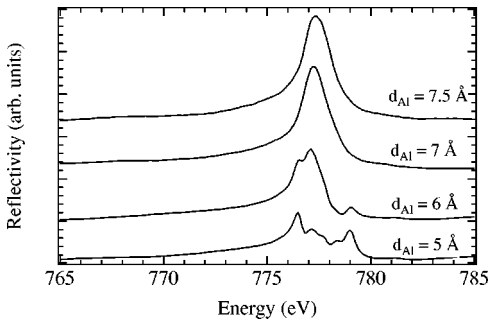

FIG. 3. X-ray resonant scattering at the Co L_3 edge measured after field annealing. Note how the data is unchanged for $d_{Al} > 7$ Å.

right-circular polarization switchable at demand at a polarization $>96\%$. Polarized x-ray techniques [x-ray magnetic circular dichroism (XMCD)[11] and x-ray resonant magnetic scattering (XRMS)[12,13]] detail changes in element specific (and therefore layer specific) magnetic and chemical properties. The samples were studied by simultaneous measurement of electron and fluorescence yields as well as reflectivity. Measurement of multiple channels provides near-surface (electron yield) and bulk (fluorescence yield) sensitivity together with interfacial structure (reflectivity). An electromagnet provides fields up to 1.5 kOe while an *e*-beam heater enabled annealing in vacuum. Samples were studied before and after an *in situ* anneal to 200 °C in a 150 Oe applied field. This way the as prepared and exchange biased structure could be studied since field annealing aligns the antiferromagnetic domains in the IrMn layer and initiates a coherent exchange bias.[14] First we examine the impact of the oxidation process on the chemical and magnetic structure of the CoFe layer, which is affected the most by the oxidation front moving past the Al spacer.

Using x-ray absorption, which is element selective and therefore in this case layer selective, can provide detailed information about the chemical and magnetic state of the separate layers. To eliminate any Co signal from the NiFeCo layer, the half junctions were used for this part of the experiment. Figure 2 contains the Co L_3 edge spectra for several Al oxide spacer thicknesses d_{Al}. Since the chemical environment strongly affects the $3d$ electrons, oxide vs metal can be easily distinguished. The oxide peak marked in Fig. 2 can be utilized to tag the oxide content and track changes as a function of field annealing and d_{Al}. For $d_{Al} < 7.5$ Å, oxygen penetrates into the CoFe layer forming an interface oxide. The field annealing reduces the content significantly. The data in Fig. 2 are from the electron yield channel and are sensitive to the top portion of the layer. Fluorescence yield shows a similar trend, but not as pronounced since it samples the whole layer equally. From the fluorescence data, the oxide content is estimated to be $\sim 20\%$ of the total film thickness (i.e., ~ 5 Å) at the thin end. Structurally the absorption is consistent with formation of Co_3O_4, which is energetically the most favorable oxide. Magnetic information from the XMCD signal shows a decrease in intensity and a lineshape consistent with the metallic portion of Co. From this we conclude that the Co_3O_4 is not ferromagnetic, which is true for the bulk but is not clear for the case of a thin layer in proximity to a ferromagnet.

While the absorption provides insight into the top portion of the CoFe layer, the TMR is still strongly sensitive to the oxidation at the $Al_2O_3/CoFe$ interface. Using x-ray reflectivity at the Co L_3 resonance, which is sensitive to the top 2–3 Å of CoFe, the chemical state at the boundary can be probed directly. Features in the energy-dependent reflectivity are also consistent with formation of oxide in the CoFe layer, but the oxide signature varies differently with d_{Al} (see Fig. 3). The oxide signature disappears around $d_{Al} = 6.5$–7 Å in marked contrast to the absorption where it occurs around 7.5–8 Å. This difference between absorption and reflectivity can be reconciled by grain boundary diffusion of the oxide. For the formation of Al_2O_3, previous studies have seen the process evolve by diffusion of oxygen around the grain and then into the grain.[3,4,8,15] Given that the layers have the same microstructure (see below) and similar energies of oxide formation, one might expect the oxidation of the ferromagnetic layer below to follow a similar course. The reflectivity is sensitive only to the $Al_2O_3/CoFe$ interface while the electron yield absorption measures the top portion of the CoFe layer. If the oxide is present first in the grain boundary, it will show clearly in the absorption. The grain boundary though comprises a small fraction of the interface and the interface signal will be dominated by the Al_2O_3/metal CoFe signature. This is also consistent with nonzero MR in the overoxidized region. Until d_{Al} is reduced to around 6 Å there are still regions of metallic CoFe in contact with Al_2O_3. The MR decreases in this region since the density/area of metal/Al_2O_3 is decreasing.[16,17]

One surprising result was that the onset of the oxidation of the CoFe layer does not start until $d_{Al} \sim 7.5$ Å, even though the optimal oxide thickness was tuned for 9 Å. Measurements of the Al *K*-edge absorption (see Fig. 4) provide insight into the electronic structure of the insulating spacer and provides an answer to this dilemma. For $d_{Al} = 9$ Å, the spectra are consistent with polycrystalline Al_2O_3. As the spacer thickness decreases, the absorption edge evolves into a second phase of Al oxide that stabilizes somewhere around 6 Å. (Note how the data for 4 and 5 Å of Al are the same.) We surmise this phase is generated by the energetic plasma oxidation of Al similar to that observed in previous studies.[3,4]

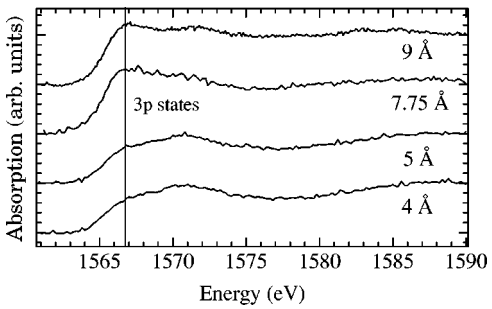

FIG. 4. Al *K* edge spectra detailing the changes due to excess oxygen in the Al_2O_3 matrix. The first peak is associated with the $3p$ density of unoccupied states.

From the edge onset it is determined that Al is still in the 3^+ oxidation state, but the decreasing intensity of the first peak (see line in Fig. 4) is attributed to a drop in the Al $3p$ density of states.[18] The excess oxygen, probably in the interstitial sites, modifies the electronic structure near the Fermi level. Since the tunneling is strongly dependent on the band structure of both the insulator and ferromagnet, the impact this type of metastable oxide would have on the TMR is uncertain.[19,20]

Next we examine the layer-specific magnetic hysteresis for the NiFeCo and CoFe layers before and after field annealing using XMCD in reflectivity (see Fig. 5). Since Ni resides only in the top layer and the bottom layer contains majority of the Co, by tuning to the Co and Ni L_3 resonances (778 and 852 eV), we can make use of the field dependent magnetic contrast to perform layer selective measurements. The measured loops are independent of d_{Al} pre- and postanneal aside from the coupling field experienced by the NiFeCo after annealing. The NiFeCo coercive field drops significantly after the anneal from 65 Oe preanneal to 20 Oe postanneal, while the CoFe layer changes from an unbiased low remanence state to a full remanence exchange biased state. The other change is the offset of the loop center with respect to zero field, which is referred to as the coupling field. The coupling field H_{coupling} experienced by the NiFeCo layer after the field annealing (see Fig. 6). H_{coupling} arises from dipolar coupling that connects the two layers resulting from the roughness of the interface (discussed below) giving rise to stray dipolar fields.[21] The behavior of H_{coupling} though is contrary to the expected exponential decay with increasing

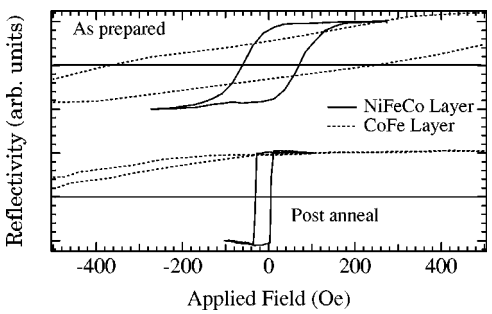

FIG. 5. Top layer (solid line) and bottom layer (dashed) hysteresis measured with element-specific x-ray reflectivity before and after field annealing.

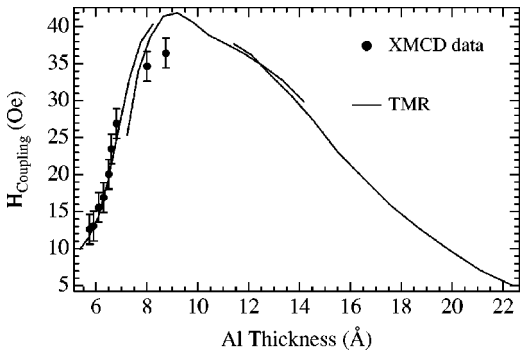

FIG. 6. Total moment magnetometry and top-layer coupling field extracted as a function of d_{Al} from the data in Fig. 5. Note the deviation from the expected decay of the coupling field with $d_{\mathrm{Al}} < 9$ Å. The overlayed TMR results show good agreement, and the expected decay for $d_{\mathrm{Al}} > 10$ Å.

d_{Al}. This results from the nonmagnetic Co_3O_4 reducing the surface magnetization and resulting dipolar fields. It also illustrates that the entire change in the NiFeCo hysteresis is attributable to dipolar exchange coupling between the two magnetic layers. Also shown in Fig. 6 is the H_{coupling} determined from TMR measurements. The results agree in the thin region and show the expected decay for $d_{\mathrm{Al}} > 10$ Å.

Since the TMR is proportional to the relative magnetic orientation of the two layers, the layer specific loops can be used to calculate a relative TMR factor.[22] Assuming the magnetization can be described by a simple rotation, the normalized moment (M/M_s) can be written as $\cos[\theta(H)]$. From the layer-specific hysteresis, one can then extract the relative orientation of the two layers $[\Delta\theta(H) = \theta_{\mathrm{NiFeCo}}(H) - \theta_{\mathrm{CoFe}}(H)]$ to calculate the relative MR factor, which is proportional to $\sin^2[\Delta\theta(H)]$. We find that the preanneal value is ~ 0.5 and increases to around ~ 0.9 after annealing. This implies that, for $d_{\mathrm{Al}} = 9$ Å, the majority of the increase in TMR is solely due to the change in the magnetic orientation of the two layers. For $d_{\mathrm{Al}} < 9$ Å the MR drops due to the increasing oxidation of the CoFe underlayer. Since the TMR factor does not change, the drop must be due to the interface oxide, which was shown above to be growing in areal density with decreasing d_{Al} until the oxide completely covers the interface ($d_{\mathrm{Al}} < 6$ Å) and TMR goes to 0.

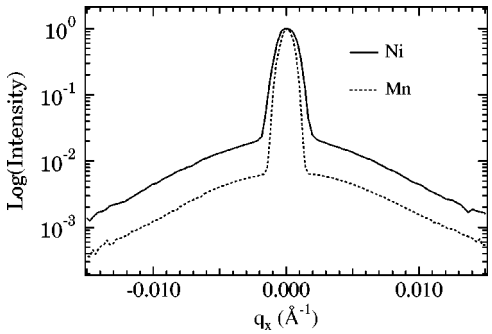

FIG. 7. X-ray resonant rocking curves at the Ni and Mn L_3 edges measured after field annealing. Both yield $\sigma = 3.2$ and $\xi = 300$ Å indicative of conformal roughness through the entire multilayer. Rocking curves are offset for clarity.

To determine that the change in TMR results from the modified dipolar interfaction between the layers and not from a decrease in the interface roughness, rocking curves were measured preannealing and postannealing.[23] By using the strong resonant enchancement of the scattering intensity, element-selective and therefore layer-specfic roughness determinations were made.[12,13] For the case of the TaN/NiFeCo and CoFe/IrMn interfaces (see Fig. 7), the sample rocking curves yield a perpendicular roughness $\sigma = \sim 3.25$ Å ± 0.5 Å and in-plane correlation length (i.e., grain size), $\xi = \sim 300$ Å ± 20 Å. These results hold for all d_{Al} both preannealing and postannealing indicating no change in the interface structure. This also indicates conformal roughness between the layers. The best fit for the shape of the diffuse scattering is for a roughness exponent of 1, which indicates a surface that varies in a smooth fashion- consistent with previous studies of polycrystalline systems.[13] The Al_2O_3/CoFe interface was examined in the half junction structure and found after annealing to have a roughness the same as the Ni and Mn interfaces. This confirms that the changes in the TMR must be magnetic and not structural in origin.

In conclusion, we have detailed changes in the layers of a magnetic tunnel junction that have been overoxidized to study the impact of unwanted oxidation. From the evidence of grain boundary diffusion, we conclude that the microstructure plays an important role in determining the impact of the oxidation process. From the perspective of TMR, the main contribution to the change with field annealing appears to be due to change in the layer dependent switching after field annealing. Since the interfacial roughness remains unchanged, it is ruled out as a factor.

Use of the Advanced Photon Source was supported by the U.S. Department of Energy, Office of Science, under Contract No. W-31-109-Eng-38. Work at Motorola Labs was supported in part by DARPA.

[1] S. A. Wolf, D. D. Awschalom, R. A. Buhrman, J. M. Daughton, S. von Molnar, M. L. Roukes, A. Y. Chtchelkanova, and D. M. Treger, Science **294**, 1488 (2001).
[2] J. S. Moodera and G. Mathon, J. Magn. Magn. Mater. **200**, 248 (1999).
[3] V. Kottler, M. F. Gillies, and A. E. T. Kuiper, J. Appl. Phys. **89**, 3301 (2001).
[4] M. F. Gillies and A. E. T. Kuiper, J. Appl. Phys. **200**, 248 (2000).
[5] D. J. Keavney, S. Park, C. M. Falco, and J. M. Slaughter, Appl. Phys. Lett. **78**, 234 (2001).
[6] L. Sevé, W. Zhu, B. Sinkovic, J. W. Freeland, I. Coulthard, W. J. Antel, Jr., and S. S. P. Parkin, Europhys. Lett. **55**, 43 (2001).
[7] M. J. Plisch, J. L. Chang, J. Silcox, and R. A. Buhrman, Appl. Phys. Lett. **79**, 391 (2001).
[8] J. S. Bae, K. H. Shin, T. D. Lee, and H. M. Lee, Appl. Phys. Lett. **80**, 1168 (2002).
[9] J. W. Freeland, J. C. Lang, G. Srajer, R. Winarski, D. Shu, and D. M. Mills, Rev. Sci. Instrum. **73**, 1408 (2001).
[10] K. J. Randall, E. Gluskin, and Z. Xu, Rev. Sci. Instrum. **66**, 4081 (1995).
[11] C. T. Chen, Y. U. Idzerda, and S. Omeone, Phys. Rev. Lett. **75**, 152 (1995).
[12] C. C. Kao, J. B. Hastings, E. D. Johnson, D. P. Siddons, and G. C. Smith, Phys. Rev. Lett. **65**, 373 (1990).
[13] J. W. Freeland, K. Bussmann, Y. U. Idzerda, and C. C. Kao, Phys. Rev. B **60**, R9923 (1999).
[14] J. van Driel, R. Coehoorn, K. M. H. Lenssen, A. E. T. Kuiper, and F. R. de Boer, J. Appl. Phys. **85**, 5522 (1999).
[15] D. J. Smith, M. R. McCartney, C. L. Platt, and A. E. Berkowitz, J. Appl. Phys. **83**, 5154 (1998).
[16] J. M. Slaughter, E. Y. Chen, R. Whig, B. N. Engel, J. Janesky, and S. Tehrani, URL http://www.tms.org/pubs/journals/JOM/0006/Slaughter/Slaughter%-0006.html
[17] S. Tehrani, B. Engel, J. M. Slaughter, E. Chen, M. DeHerrera, M. Durlam, P. Naji, R. Whig, J. Janesky, and J. Calder, IEEE Trans. Magn. **36**, 2752 (2000).
[18] P. Ildefonse, D. Cabaret, P. Sainctavit, G. Calas, A. M. Flank, and P. Lagarde, Phys. Chem. Miner. **25**, 112 (1998).
[19] E. Y. Tsymbal and D. G. Pettifor, J. Phys.: Condens. Matter **9**, L411 (1997).
[20] J. M. MacLaren, X. G. Zhang, and W. H. Butler, Phys. Rev. B **56**, 11 827 (1997).
[21] S. Tegen, I. Monch, J. Schumann, H. Vinzelberg, and C. M. Schneider, J. Appl. Phys. **89**, 8169 (2001).
[22] Y. U. ldzerda, C. T. Chen, S. F. Cheng, W. Vavra, G. A. Prinz, G. Meigs, H. J. Lin, and G. H. Ho, Appl. Phys. Lett. **64**, 3503 (1994).
[23] S. K. Sinha, E. B. Sirota, S. Garoff, and H. B. Stanley, Phys. Rev. B **38**, 2297 (1988).